A Novel All-Digital Calibration Method for Timing Mismatch in Time-Interleaved ADC Based on Modulation Matrix

Sujuan Liu, *Member, IEEE*, Lin Zhao, and Shibo Li

***Abstract*— This paper proposes a novel all-digital background calibration of timing mismatch for a time-interleaved analog-to-digital converter (TIADC). For two different calibration strategies, the absolute calibration and the relative calibration, the inductive expressions of modulation matrices are derived from the coefficient matrices provided by different estimation methods. Based on the modulation matrix, we develop a digital calibration architecture, which enables the output of TIADC to be modulated firstly before being corrected, so the costly matrix multiplication processing can be avoided. This calibration architecture also enables the estimation process of each channel to be independent and can be executed simultaneously, which accelerates the convergence speed of the timing mismatch. We show the efficiency of the calibration structure by simulations, including examples from the literature. Numerical simulation demonstrates that the convergence speed of the timing mismatch has been improved by at least 27%, compared with the estimation method depending on the specified reference channel. The result of FPGA-based hardware implementation shows that the spurious-free dynamic range (SFDR) is improved by 37.63dB.**

***Index Terms*— Time-interleaved ADC, background calibration, blind estimation, timing mismatch.**

I. Introduction

ANALOG-TO-DIGITAL converter (ADC) can convert analog signals into digital signals, which play an important role in modern communication systems. Wireless communication systems, measuring instruments and other fields have higher and higher performance requirements for ADCs, but traditional ADCs are increasingly difficult to meet the demand. In order to achieve a high-speed and high-resolution ADC, a time-interleaved structure is adopted. The time-interleaved analog-to-digital converter (TIADC) uses M ADCs to sample alternately. Ideally, the overall sampling rate is M times the sampling rate of a single ADC, and the resolution is the same as that of a single ADC. However, due to manufacturing differences and changes in voltage or temperature, the characteristics of each ADC will be different, which can cause mismatches between channels, such as offset, gain and timing mismatches. These mismatches will reduce the system performance of TIADC [1], such as Signal-to-Noise Ratio (SNR), Spurious-Free Dynamic Range (SFDR). In order to improve the performance of TIADC, these mismatches need to be calibrated. Gain and offset mismatches are relatively straightforward to calibrate because their powers are independent of the input frequency. Therefore, the offset and gain mismatches can be estimated by averaging each sub-ADC output and correcting them in the digital domain directly [2]–[4]. However, the power of errors caused by timing mismatch increases with the input frequency, thus presenting a greater challenge and becoming a dominant issue in TIADCs, which is the calibration focus of this work.

In the calibration structure of TIADC, compared to analog compensation methods such as variable delay lines [5], [6], the all-digital calibration method is not easily affected by the process, voltage and temperature [7]. Therefore, this paper focuses on the all-digital calibration of timing mismatch.

In digital calibration, the foreground calibration method requires a reference signal [8] or interrupting TIADC work to complete the calibration. However, the background calibration method can be completed during ADC operation, so it is more attractive [9]. In the digital domain, finite impulse response (FIR) filters such as differentiators [10]–[14], fractional delay filters [15], and filter bank [16] are often used to complete compensation. Tertinek and Vogel [10] proposed a method of compensation using a differentiator [14] and modulation signal. Based on this method, the high-pass filter and a least-mean-square (LMS) [17] algorithm can be used to estimate the timing mismatch [18], [19] and complete the adaptive blind calibration. However, this estimation method limits the bandwidth of the input signal and requires a lot of hardware resources [20]. Both the Hadamard transform [12] and the Hilbert transform [13] can be used to reconstruct the error signal, and use a differentiator to calibrate the timing mismatch of each channel. These methods all calibrate the timing mismatch to the average of all timing mismatches.

In [21], the delta sampling auxiliary SAR ADCs and the digital-mixing calibration technique are employed to compensate timing mismatch. This approach needs an extra analog auxiliary circuit to estimate the mismatch errors and the additional channels required for the calibration add power or area overheads. The input impedance of the overall ADC is changing because of the reference channel, which is an issue for high-speed ADCs. To overcome the dynamic settling error

Manuscript received December 7, 2021; revised March 2, 2022; accepted March 19, 2022. Date of publication April 11, 2022; date of current version June 29, 2022. This work was supported in part by the National Natural Science Foundation of China under Grant 62074010. This article was recommended by Associate Editor P. K. Meher. *(Corresponding author: Sujuan Liu.)*

The authors are with the College of Microelectronics, Beijing University of Technology, Beijing 100124, China (e-mail: liusujuan@bjut.edu.cn; zl573589086@163.com; lishibo98@emails.bjut.edu.cn).

Color versions of one or more figures in this article are available at https://doi.org/10.1109/TCSI.2022.3163431.

Digital Object Identifier 10.1109/TCSI.2022.3163431

caused by the reference channel, the split TI architecture is proposed in [4], where a conventional TIADC is split into two mutual prime numbers parts. Similar to [4], a relative-prime-based TI (RP TI) sub-ranging SAR ADC is proposed in [22]. The idea of [22] is also based on the reference channel calibration and the relative-prime concept. However, this method is applicable for the specific architectures not suitable for common TIADCs architectures.

The statistical characteristics of the signal can be used to estimate the timing mismatch [6], [23]–[30]. The estimation method in [6], [24], [25] can estimate the difference between the timing mismatches of adjacent channels. The timing mismatch detection technique based on autocorrelation function is proposed for two-channel TIADC in [5]. However, the complexity for estimation increases when the concept is extended to multiple channels. Estimation methods that do not require digital multipliers have been proposed to reduce complexity [32], but the calibration process requires to be divided into several steps and be corrected step by step [26]. Every two channels are set as a group, the next group can be started only after the previous group is corrected. This step-by-step calibration makes the estimation process of each channel interdependent, which will slow down the convergence speed. And the number of channels is strictly limited to the power of 2. In our previous work [27], we also use a similar idea to calibrate the TIADC step by step.

For four or more channels, the pseudo-inverse matrix can be used to obtain the error coefficient [28]–[30] to make the estimation process independent. And the differentiator is used to calibrate the timing mismatch of each channel to an average value. When using the pseudo-inverse matrix to estimate the mismatch, the timing mismatch of each channel needs to be obtained by multiplying the estimation result and the pseudo-inverse matrix. This process will increase the amount of calculation, and the more channels there are, the greater the number of computations.

Therefore, this paper proposes a new calibration method based on the modulation matrix, which can avoid the multiplication of the pseudo-inverse matrix with the iterative result and improve the error convergence speed of the estimation method based on the statistical characteristics between adjacent channels. The contribution of our work mainly has three parts.

Our main contribution is to deduce the inductive expressions of the calibration method based on the concepts of the modulation matrix and the coefficient matrix, which can be used to guide the design of TIADC calibration. For two different calibration strategies, the absolute calibration and the relative calibration, we derive the inductive expressions of modulation matrices that are corresponding to the coefficient matrices provided by different estimation methods. And the timing mismatch can be calibrated to approximately zero, or to the average value of all channel timing mismatches, or the same as that of the reference channel. Namely, we aim to conclude a calibration method that has the ability to correct the timing mismatches for any channel TIADC with different estimation methods.

Our second contribution is a digital architecture based on the modulation matrix which enables avoiding the multiplication of the pseudo-inverse matrix and the estimation result for the application that the timing mismatch of each channel cannot be obtained directly. The derivative output of TIADC is modulated by the modulation matrix before correction, and the correction can be carried out without obtaining the value of timing mismatch of each channel. For the implementation of this architecture, only a simple shift operation is required for the modulation matrix, which reduces the hardware complexity considerably compared with costly matrix multiplication processing.

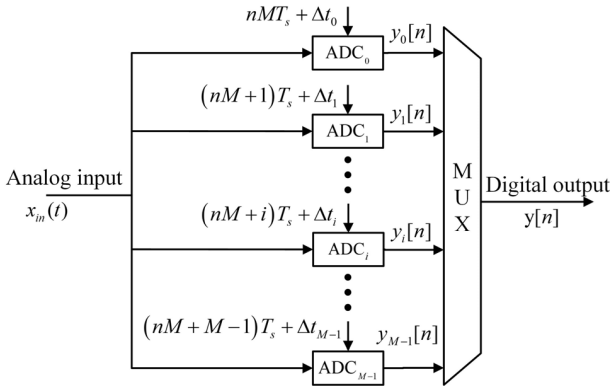

Fig. 1. Schematic implementation of an M channels TIADC.

In addition, this calibration architecture also enables the estimation process of each channel to be independent and allows them to be executed synchronously and independently. It accelerates the convergence speed of the timing mismatch, in contrast to the methods which permit every two channels to be calibrated step by step through setting the specified reference channel. We also derived the requirements for the estimation module when using this calibration architecture.

This paper is organized as follows. Section II introduces the TIADC model and system analysis. In Section III, we describe the proposed calibration architecture and provide a theoretical analysis of the calibration method based on the concepts of the modulation matrix and the coefficient matrix. Section IV describes the used estimation method. The simulation results and hardware implementation are presented in Section V. Concluding remarks are finally drawn in Section VI.

II. System Model Analysis

The schematic implementation of TIADC with M channels is shown in Fig. 1, where the analog input signal $x_{in}(t)$ is alternately sampled by M sub-ADCs (ADC_0 to ADC_{M-1}) with a sampling rate of f_s/M in the time-multiplexing fashion, and therefore the TIADC operates at a sampling rate of f_s. The sampling interval is T_s ($T_s = 1/f_s$), and Δt_i $(0 \le i \le M-1)$ represents the value of the timing mismatch of the i-th channel. The output $y_i[n]$ of each sub-ADC is combined into the output $y[n]$ of TIADC after passing through the multiplexer (MUX).

In this paper, offset mismatch and gain mismatch are not taken into account. For simplicity, we focus on the calibration of timing mismatch and assume that the offset mismatch and the gain mismatch are calibrated separately. According to

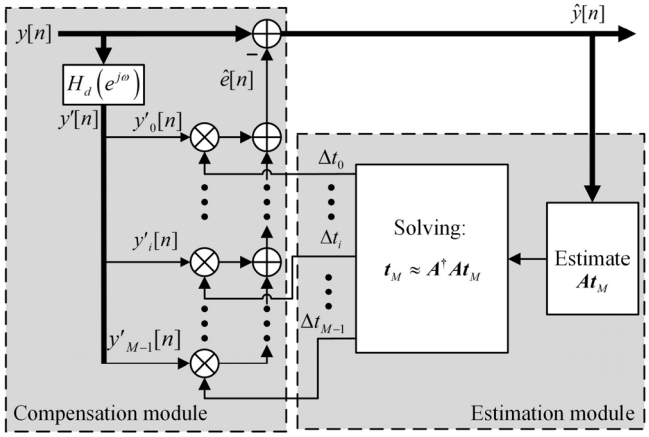

Fig. 2. The general calibration structure.

Fig. 1, the output of the i-th channel of TIADC is [6]

$$y_i[n] = \begin{cases} x_{in}((nM+i)T_s + \Delta t_i), & i = n \bmod M \\ 0, & else \end{cases} \quad (1)$$

By the first-order Taylor expansion, (1) can be expanded as

$$y_i[n] \approx x_i[n] + \Delta t_i x_i'[n] \quad (2)$$

where $x_i[n]$ represents the input of the i-th channel, and

$$x_i[n] = \begin{cases} x_{in}((nM+i)T_s), & i = n \bmod M \\ 0, & else \end{cases} \quad (3)$$

where $x_i'[n]$ is the first-order derivative of the i-th input signal $x_i[n]$ at the nominal sampling time which can be obtained by a derivative filter. After passing through the multiplexer (MUX), the output $y[n]$ of TIADC is represented by

$$y[n] \approx x[n] + \sum_{i=0}^{M-1} \Delta t_i x_i'[n]. \quad (4)$$

The error signal $e[n]$ caused by the timing mismatch can be defined as

$$e[n] = \sum_{i=0}^{M-1} \Delta t_i x_i'[n]. \quad (5)$$

For our purposes, it is convenient to write (5) in matrix form as

$$e[n] = \boldsymbol{x}_{\boldsymbol{d},\boldsymbol{M}}^T \boldsymbol{t_M} \quad (6)$$

where, $\boldsymbol{x_{d,M}}$ is a vector of length M with i-th element $x_i'[n]$ being the derivative of $x_i[n]$ and can be expressed as

$$\boldsymbol{x_{d,M}} = \left[x_0'[n], \ldots, x_i'[n], \ldots, x_{M-1}'[n]\right]^T \quad (7)$$

and, $\boldsymbol{t_M}$ is a vector of length M with i-th element Δt_i being the timing mismatch of the i-th channel and can be expressed as

$$\boldsymbol{t_M} = \left[\Delta t_0, \ldots, \Delta t_i, \ldots, \Delta t_{M-1}\right]^T \quad (8)$$

where $[\cdot]^T$ represents transpose.

If the timing mismatch Δt_i of each channel can be estimated, it can be multiplied by the derivative of the input signal to reconstruct the error signal $e[n]$. The calibration structure based on the above analysis is described in Fig. 2, where $H_d(e^{j\omega})$ represents the differentiator. The timing mismatch of each channel can be obtained through the estimation module. Since $x[n]$ cannot be obtained, we use $y[n]$ to replace it [28], [30]. And $y_i'[n]$ represents the first-order derivative of the output of the i-th channel. Assuming that the reconstruction error signal is $\hat{e}[n]$, the output after compensation $\hat{y}[n]$ is expressed as

$$\hat{y}[n] = y[n] - \hat{e}[n] \approx x[n] + e[n] - \hat{e}[n]. \quad (9)$$

For most estimation modules, Δt_i cannot be directly obtained, instead, a linear combination of Δt_i can be obtained easier. By separating the coefficients of the linear combination and Δt_i, the estimation result can be expressed in the form of a matrix as $\boldsymbol{At_M}$, where $\boldsymbol{A}$ is the coefficient matrix formed by the linear combination coefficients and $\boldsymbol{t_M}$ represents the vector of timing mismatch.

In the previous research [28]–[30], it is necessary to calculate the pseudo-inverse matrix ($\boldsymbol{A}^{\dagger}$) of the coefficient matrix $\boldsymbol{A}$, as shown in the estimation module in Fig. 2. The timing mismatch Δt_i of each channel can be obtained by multiplying the estimation result by the pseudo-inverse matrix. According to (6) and (9), if the reconstruction error signal $\hat{e}[n]$ is calibrated to approximately 0, then $\hat{e}[n] \approx e[n]$ is required, and $\hat{e}[n]$can be expressed as

$$\hat{e}[n] \approx e[n] \approx \boldsymbol{y}_{\boldsymbol{d},\boldsymbol{M}}^T \boldsymbol{t_M} \approx \boldsymbol{y}_{\boldsymbol{d},\boldsymbol{M}}^T \boldsymbol{A}^{\dagger} \boldsymbol{A t_M} \quad (10)$$

where $\boldsymbol{y_{d,M}} = \left[y_0'[n], \ldots, y_i'[n], \ldots, y_{M-1}'[n]\right]^T$ is a column vector of length M with i-th element $y_i'[n]$ being the derivative of $y_i[n]$.

For this calibration method, as the number of channels increases, the computational complexity will increase simultaneously. Hence, in the next section, we introduce the concept of modulation matrix to avoid multiplying the pseudo-inverse matrix with the estimation result.

III. Proposed Calibration Method

Before introducing the modulation matrix, it is necessary to classify the calibration strategies. According to (9) and the analysis in Section I, it can be inferred that there are two calibration strategies, which are divided into absolute calibration and relative calibration. The absolute calibration is used to compensate the timing mismatch of each channel to approximately zero. The relative calibration means that the timing mismatch of each channel is compensated to the same value, which is equivalent to an overall delay of the input signal. The relative calibration does not affect performance. The mathematical derivation of the modulation matrix of the two different calibration strategies is different.

A. Modulation Matrix for Absolute Calibration

Since $\boldsymbol{t_M}$ cannot be obtained directly from the estimation module, we need to use the coefficient matrix in (10) to

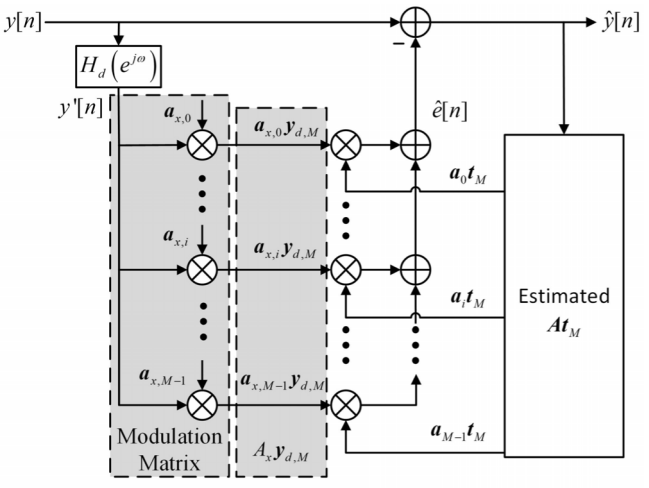

Fig. 3. The proposed absolute calibration architecture.

derive the calibration method. According to (9), if the error is calibrated to approximately 0, then $\hat{e}[n] \approx e[n]$ is required, so $\hat{e}[n]$ can be rewritten as

$$\hat{e}[n] \approx \boldsymbol{y}_{\boldsymbol{d},\boldsymbol{M}}^{T}\boldsymbol{t_M} = \boldsymbol{y}_{\boldsymbol{d},\boldsymbol{M}}^{T}\boldsymbol{I}\boldsymbol{t_M} \tag{11}$$

where $\boldsymbol{I}$ is the identity matrix of size $M \times M$. If there are matrices $\boldsymbol{A_x}$ and $\boldsymbol{A}$, make

$$\boldsymbol{A}_{\boldsymbol{x}}^{T}\boldsymbol{A} = \boldsymbol{I} \tag{12}$$

then (11) can be rewritten as

$$\hat{e}[n] = \left(\boldsymbol{A_x}\boldsymbol{y_{d,M}}\right)^{T}\boldsymbol{At_M} \tag{13}$$

where $\boldsymbol{A_x}$ is defined as the modulation matrix for absolute calibration. And $\boldsymbol{A}$ is the coefficient matrix of the linear combination of Δt_0 to Δt_{M-1}. Based on the modulation matrix, the proposed absolute calibration architecture is schematically drawn in Fig. 3 with its estimated result $\boldsymbol{At_M}$.

As depicted in Fig. 3, if matrix $\boldsymbol{A_x} = [\boldsymbol{a}_{x,0}, \ldots, \boldsymbol{a}_{x,i}, \ldots, \boldsymbol{a}_{x,M-1}]^T$, and $\boldsymbol{a}_{x,i} = [a_{i,0}, \ldots, a_{i,j}, \ldots, a_{i,M-1}]^T, 0 \le i \le M-1,\ 0 \le j \le M-1$, where $\boldsymbol{a}_{x,i}$ is the i-th row of the matrix $\boldsymbol{A_x}$, and $a_{i,j}$ is the j-th element of the i-th row of the modulation matrix $\boldsymbol{A_x}$, then $\boldsymbol{A_x}\boldsymbol{y_{d,M}}$ can be understood in implementation as modulating $y'[n]$ with each row $\boldsymbol{a_{x,i}}$ of the matrix $\boldsymbol{A_x}$. Since the matrix $\boldsymbol{A_x}$ has M rows, $\boldsymbol{y_{d,M}}$ needs to be modulated for M times. The modulation matrix $\boldsymbol{A_x}$ can be obtained by (12)

$$\boldsymbol{A_x} = \left(\boldsymbol{A^{-1}}\right)^{\boldsymbol{T}}. \tag{14}$$

According to (13) and (14), if $\boldsymbol{t_M}$ cannot be obtained directly by the estimation module, we can modulate $y'[n]$ through the modulation matrix $\boldsymbol{A_x}$, and then multiply it by the estimated $\boldsymbol{At_M}$ for reconstructing the error signal $e[n]$. Finally, the reconstruction error signal $\hat{e}[n]$ can be subtracted from the TIADC output signal $y[n]$ to obtain the calibrated signal $\hat{y}[n]$, as shown in Fig. 3. The linear combination of Δt_i for the i-th channel $\boldsymbol{a_i t_M}$ can be obtained from the estimation module, where, $\boldsymbol{a}_i$ is the i-th row of the coefficient matrix $\boldsymbol{A}$.

B. Modulation Matrix for Relative Calibration

If the coefficient matrix obtained from the estimation module is not full rank, the absolute calibration strategy cannot be used because the identity matrix $\boldsymbol{I}$ in (12) cannot be constructed from the coefficient matrix and the modulation matrix. But the relative calibration can be used to deal with this situation. In practice, there is no need to compensate the timing mismatch of each channel to approximately zero. We only need to calibrate the timing error of each channel to be the same value, which achieves the goal of "no mismatch" between the channels of TIADC. That is sufficient for most applications because the same timing mismatch of each channel is equivalent to an overall delay of the input signal. In fact, the relative calibration has the advantage in terms of practical implementation. From the analysis in the previous section, we need to construct the reconstruction error signal $\hat{e}[n]$ similar to (11) for using the coefficient matrix to find the modulation matrix. The relative calibration can be divided into two cases. The first case is that the timing mismatch of each channel is compensated to the average of all channel timing mismatches. The second case is that after a certain channel is selected as a reference channel, the timing mismatches of the remaining channels are compensated to that of the reference channel. Firstly, we describe the first case.

1) The First Case: If the timing mismatch of each channel is not calibrated to absolute 0 but the average of all channel timing mismatches, i.e., the residual $\Delta\hat{t}_i = (\Delta t_0 + \Delta t_1 + \ldots + \Delta t_{M-1})/M$. Then the residual vector $\hat{\boldsymbol{t}}_{\boldsymbol{M}} = \left[\Delta\hat{t}_0, \ldots, \Delta\hat{t}_i, \ldots, \Delta\hat{t}_{M-1}\right]^T$ can be expressed as

$$\hat{\boldsymbol{t}}_{\boldsymbol{M}} = \boldsymbol{\Gamma}\boldsymbol{t_M} \tag{15}$$

where, $\boldsymbol{\Gamma}$ is convenient to define in matrix form as

$$\boldsymbol{\Gamma} = \frac{1}{M}\begin{bmatrix} 1 & \cdots & 1 \\ \vdots & \ddots & \vdots \\ 1 & \cdots & 1 \end{bmatrix}. \tag{16}$$

Because the objective function of the calibration is the average of all channel timing mismatches, so the difference between the reconstruction error signal $\hat{e}[n]$ and the error signal $e[n]$ in (6) is given by

$$e[n] - \hat{e}[n] = \boldsymbol{x}_{\boldsymbol{d},\boldsymbol{M}}^{T}\hat{\boldsymbol{t}}_{\boldsymbol{M}} = \boldsymbol{x}_{\boldsymbol{d},\boldsymbol{M}}^{T}\boldsymbol{\Gamma}\boldsymbol{t_M}. \tag{17}$$

Substitute (6) into (17), replace $\boldsymbol{x_{d,M}}$ with $\boldsymbol{y_{d,M}}$, and get

$$\hat{e}[n] = \boldsymbol{y}_{\boldsymbol{d},\boldsymbol{M}}^{T}(\boldsymbol{I} - \boldsymbol{\Gamma})\boldsymbol{t_M} \tag{18}$$

where $\boldsymbol{I} - \boldsymbol{\Gamma}$ is an $M \times M$ matrix, with the elements calculated by (16). $\boldsymbol{I} - \boldsymbol{\Gamma}$ can be written in matrix form as

$$\boldsymbol{I} - \boldsymbol{\Gamma} = \begin{bmatrix} 1 - \frac{1}{M} & -\frac{1}{M} & \cdots & -\frac{1}{M} \\ -\frac{1}{M} & 1 - \frac{1}{M} & \cdots & -\frac{1}{M} \\ \vdots & \vdots & \ddots & \vdots \\ -\frac{1}{M} & -\frac{1}{M} & \cdots & 1 - \frac{1}{M} \end{bmatrix}. \tag{19}$$

Equation (18) shows that if there are matrix $\boldsymbol{B}$ and matrix $\boldsymbol{B_x}$, and

$$\boldsymbol{B_x^T B} = \boldsymbol{I} - \boldsymbol{\Gamma} \tag{20}$$

then the reconstruction error signal $\hat{e}[n]$ can be reconstructed by $\left(\boldsymbol{B_x y_{d,M}}\right)^T \boldsymbol{B t_M}$, where $\boldsymbol{B}$ and $\boldsymbol{B_x}$ respectively represent the coefficient matrix and the modulation matrix for relative calibration. The same as the analysis in the section III-A, the modulation matrix $\boldsymbol{B_x}$ needs to be solved by using (20). After performing the elementary transformation on $\boldsymbol{I} - \boldsymbol{\Gamma}$, the rank of $\boldsymbol{I} - \boldsymbol{\Gamma}$ can be obtained as $M - 1$. So, the matrix $\boldsymbol{B_x}$ and matrix $\boldsymbol{B}$ need to be restricted, namely

$$rank(\boldsymbol{I}-\boldsymbol{\Gamma}) = rank(\boldsymbol{B_x^T B}) = M-1 \leq min(rank(\boldsymbol{B_x^T}), rank(\boldsymbol{B})). \tag{21}$$

Therefore, the ranks of the matrices $\boldsymbol{B_x}$ and $\boldsymbol{B}$ cannot be less than $M-1$. However, in the relative calibration, the coefficient matrix $\boldsymbol{B}$ is not full rank, so the rank of the coefficient matrix $\boldsymbol{B}$ is equal to $M-1$, and the size is $(M-1) \times M$. If the size of the obtained coefficient matrix $\boldsymbol{B}$ is $M \times M$, one row can be discarded. Assuming that the estimated coefficient matrix $\boldsymbol{B}$ is known, (20) can be used to find $\boldsymbol{B_x}$. Since the rank of the coefficient matrix $\boldsymbol{B}$ is not equal to M, and $\boldsymbol{I}-\boldsymbol{\Gamma}$ is not a full-rank matrix, we need to use the pseudo-inverse matrix to get $\boldsymbol{B_x}$. Since $\boldsymbol{B}$ is a $(M-1) \times M$ matrix, there is a right inverse, i.e., $\boldsymbol{B B^\dagger} = \boldsymbol{I}$, $[\cdot]^\dagger$ represents a pseudo-inverse matrix, and

$$\boldsymbol{B^\dagger} = \boldsymbol{B^T}\left(\boldsymbol{B B^T}\right)^{-1}. \tag{22}$$

According to (20),

$$\boldsymbol{B_x^T} = (\boldsymbol{I} - \boldsymbol{\Gamma})\,\boldsymbol{B^\dagger} \tag{23}$$

and

$$\boldsymbol{B_x} = \left((\boldsymbol{I} - \boldsymbol{\Gamma})\,\boldsymbol{B^\dagger}\right)^{\boldsymbol{T}}. \tag{24}$$

It can be seen from (24) that the size of the modulation matrix $\boldsymbol{B_x}$ is the same as the coefficient matrix $\boldsymbol{B}$. Since the pseudo-inverse matrix only has the property of an inverse matrix, the identity matrix cannot be obtained by multiplying the pseudo-inverse matrix with the original matrix. In order to verify whether the result is correct, substitute (24) into (20) to obtain

$$(\boldsymbol{I} - \boldsymbol{\Gamma})\,\boldsymbol{B^\dagger B} = (\boldsymbol{I} - \boldsymbol{\Gamma}). \tag{25}$$

Since $\boldsymbol{B^\dagger}$ is the right inverse matrix of $\boldsymbol{B}$, not all matrix $\boldsymbol{B}$ with rank $M-1$ can make (25) true, so we need to restrict matrix $\boldsymbol{B}$. If the right term in (25) is moved to the left, the following equation can be obtained

$$(\boldsymbol{I} - \boldsymbol{\Gamma})\left(\boldsymbol{B^\dagger B} - \boldsymbol{I}\right) = \boldsymbol{O} \tag{26}$$

where $\boldsymbol{O}$ represents a matrix with all zero elements. Then the matrix $\boldsymbol{B}$ can be restricted by solving the homogeneous linear equations $(\boldsymbol{I} - \boldsymbol{\Gamma})\,\boldsymbol{x} = \boldsymbol{0}$ [31]. It can be seen from (19) that the rank of $\boldsymbol{I} - \boldsymbol{\Gamma}$ is $M-1$, and the sum of row elements is equal to 0, then the general solution of $(\boldsymbol{I} - \boldsymbol{\Gamma})\,\boldsymbol{x} = \boldsymbol{0}$ is

$$\boldsymbol{x} = k\begin{bmatrix} 1 & 1 & \cdots & 1 \end{bmatrix}^T \tag{27}$$

where $\boldsymbol{x}$ is a vector of length M with all elements k and k is an arbitrary constant. According to (26), the column vectors in $\boldsymbol{B^\dagger B - I}$ are all solutions of $(\boldsymbol{I} - \boldsymbol{\Gamma})\,\boldsymbol{x} = \boldsymbol{0}$, then

$$\boldsymbol{B^\dagger B - I} = \begin{bmatrix} k_1 & k_2 & \cdots & k_M \\ k_1 & k_2 & \cdots & k_M \\ \vdots & \vdots & \cdots & \vdots \\ k_1 & k_2 & \cdots & k_M \end{bmatrix} \tag{28}$$

where k_1 to k_M are arbitrary constants. Therefore, in the relative calibration, the elements in each column of the matrix $\boldsymbol{B^\dagger B - I}$ must be the same.

2) The Second Case: The expression of the reconstruction error signal $\hat{e}[n]$ in the second case is similar to (18). The difference is that one of the TIADC channels is used as the reference channel, and the timing mismatches of the remaining channels are compensated to be the same as that of the reference channel. Then the reconstruction error signal is defined as

$$\hat{e}[n] = \boldsymbol{y_{d,M}^T}\,(\boldsymbol{I} - \boldsymbol{D})\,\boldsymbol{t_M}. \tag{29}$$

If the remaining channels are compensated to have the same timing mismatch as the i-th channel, the elements in the i-th column of the $M \times M$ matrix $\boldsymbol{D}$ are all 1, and the remaining columns are all 0. Take the first channel as an example, the $M \times M$ matrix $\boldsymbol{D}$ in this setting can be written as

$$\boldsymbol{D} = \begin{bmatrix} 1 & 0 & \cdots & 0 \\ 1 & 0 & \cdots & 0 \\ \vdots & \vdots & \ddots & \vdots \\ 1 & 0 & \cdots & 0 \end{bmatrix} \tag{30}$$

and

$$\boldsymbol{I} - \boldsymbol{D} = \begin{bmatrix} 0 & 0 & 0 & \cdots & 0 \\ -1 & 1 & 0 & \cdots & 0 \\ -1 & 0 & 1 & 0 & 0 \\ \vdots & \vdots & \vdots & \ddots & \vdots \\ -1 & 0 & 0 & \cdots & 1 \end{bmatrix}. \tag{31}$$

The rank of the $M \times M$ matrix $\boldsymbol{I} - \boldsymbol{D}$ is also $M-1$, and the sum of the row elements is also 0, so the requirements for the modulation matrix and the coefficient matrix of the second case are the same as those of the first case. The solving process of the modulation matrix $\boldsymbol{B_x}$ is also the same as the first case, which is

$$\boldsymbol{B_x} = \left((\boldsymbol{I} - \boldsymbol{D})\,\boldsymbol{B^\dagger}\right)^{\boldsymbol{T}}. \tag{32}$$

From the above analysis and derivation, it can be known that for the relative calibration, two restrictions on the coefficient matrix $\boldsymbol{B}$ are required:

- The rank of the coefficient matrix $\boldsymbol{B}$ is $M-1$;
- The elements in each column of $\boldsymbol{B^\dagger B - I}$ have the same value.

Only when these two conditions are met can the relative calibration be performed.

The proposed relative calibration architecture is shown in Fig. 4. And $\boldsymbol{b_i}$ represents the i-th row of the coefficient matrix $\boldsymbol{B}$, and $\boldsymbol{b_{x,i}}$ represents the i-th row of the coefficient

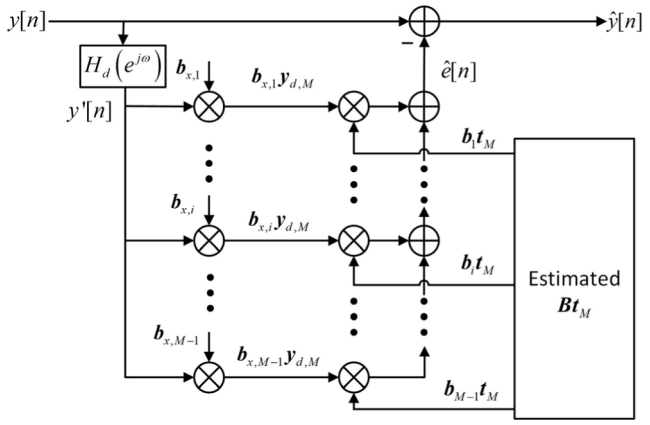

Fig. 4. The proposed relative calibration architecture.

matrix $\boldsymbol{B_x}$. The modulated derivative signal $\boldsymbol{B_x y_{d,M}}$ is multiplied by the estimation result $\boldsymbol{Bt_M}$ to obtain the reconstruction error signal $\hat{e}[n]$. Compared with Fig. 3, the relative calibration only needs to estimate the linear combination of $M-1$ kinds of Δt_i, i.e., $\boldsymbol{b}_1\boldsymbol{t_M}$ to $\boldsymbol{b}_{M-1}\boldsymbol{t_M}$ in Fig.4. So, the relative calibration outperforms the absolute calibration in practical implementation.

In the previous analysis, we assumed that the coefficient matrix $\boldsymbol{A}$ and $\boldsymbol{B}$ is known, but in practice, we need to obtain $\boldsymbol{A}$ and $\boldsymbol{B}$ through some estimation methods. The estimation methods based on the correlation function [5], [28], [29] and the statistical characteristics between adjacent channels [6], [24]–[26], [30] are widely used, and the coefficient matrices obtained by these two estimation methods satisfy all the requirements of our problem formulation in (21) and (28) for the relative calibration cases. Therefore, for the proposed calibration structure, these two estimation methods can be used to obtain the coefficient matrix $\boldsymbol{B}$. How to get the coefficient matrix $\boldsymbol{B}$ will be explained in the next section.

IV. Estimation Module

Estimating the error utilizing the correlation function or the statistical characteristics between adjacent channels will result in a coefficient matrix with rank $M-1$. Take the estimation method based on the correlation function as an example, and assume that the input signal is a Wide-Sense Stationary (WSS) signal. We define $E[\cdot]$ as the mean value, $R_{l,g}(m)$ as the cross-correlation function, and define

$$R_{l,g}(m) = E[l[n]\, g[n+m]]. \tag{33}$$

According to (1) and (33), the correlation function of the i-th channel and the $(i+1)$-th channel at $m=0$ is

$$\begin{aligned} R_{y_i,y_{i+1}}(0) &= E\left[y_i[n]\, y_{i+1}[n]\right] \\ &= E[x((nM+i)T_s + \Delta t_i) \\ &\quad \cdot x((nM+i)T_s + T_s + \Delta t_{i+1})\big] \\ &= R_{x_i,x_i}(T_s + \Delta t_{i+1} - \Delta t_i). \end{aligned} \tag{34}$$

At $m = T_s$, the first-order Taylor expansion of (34) can be obtained

$$\begin{aligned} R_{x_i,x_i}(T_s+\Delta t_{i+1}-\Delta t_i) &\approx R_{x_i,x_i}(T_s) \\ &\quad + (\Delta t_{i+1}-\Delta t_i) R'_{x_i,x_i}(T_s). \end{aligned} \tag{35}$$

Similarly, $R_{y_{i-1},y_i}(0) = R_{x_i,x_i}(T_s + \Delta t_i - \Delta t_{i-1})$. The difference τ_i of the two correlation functions is defined as

$$\begin{aligned} \tau_i &= R_{y_{i-1},y_i}(0) - R_{y_i,y_{i+1}}(0) \\ &= R_{x_i,x_i}(T_s + \Delta t_i - \Delta t_{i-1}) - R_{x_i,x_i}(T_s + \Delta t_{i+1} - \Delta t_i) \\ &\approx R'_{x_i,x_i}(T_s)(-\Delta t_{i-1} + 2\Delta t_i - \Delta t_{i+1}) \end{aligned} \tag{36}$$

where $1 \le i \le M-1$. Define $\boldsymbol{\tau}$ as $\left[\tau_1, \ldots, \tau_i, \ldots, \tau_{M-1}\right]^T$. According to (36), for our calibration, it is convenient to write $\boldsymbol{\tau}$ in matrix form as

$$\boldsymbol{\tau} = R'_{x_i,x_i}(T_s)\, \boldsymbol{Bt_M} \tag{37}$$

where $\boldsymbol{B}$ is the defined coefficient matrix with a size of $(M-1)\times M$, and the elements in the i-th row of it are obtained from the coefficient of the linear combination of Δt_{i-1}, Δt_i and Δt_{i+1} in (36). The elements of the other rows of $\boldsymbol{B}$ are the shift copies of that of the i-th row, so $\boldsymbol{B}$ can be expressed in matrix form as

$$\boldsymbol{B} = \begin{bmatrix} -1 & 2 & -1 & 0 & \cdots & 0 & 0 \\ 0 & -1 & 2 & -1 & \cdots & 0 & 0 \\ \vdots & \vdots & \vdots & \vdots & \vdots & \vdots & \vdots \\ -1 & 0 & 0 & 0 & \cdots & -1 & 2 \end{bmatrix} \tag{38}$$

and the rank of $\boldsymbol{B}$ is $M-1$. Since $R'_{x_i,x_i}(T_s)$ is a constant, to estimate the value of the linear combination of timing error $\boldsymbol{Bt_M}$, the iterative algorithm is applied to (36) and (37) using multipliers and accumulators, i.e.,

$$(\boldsymbol{Bt_M})^{(n+1)} = (\boldsymbol{Bt_M})^{(n)} + \mu\boldsymbol{\tau} \tag{39}$$

and according to (28) and (38),

$$\boldsymbol{B}^{\dagger}\boldsymbol{B} - \boldsymbol{I} = -\frac{1}{M}\begin{bmatrix} 1 & \cdots & 1 \\ \vdots & \ddots & \vdots \\ 1 & \cdots & 1 \end{bmatrix}. \tag{40}$$

The coefficient matrix $\boldsymbol{B}$ satisfies the two conditions described in section III. Therefore, the relative calibration method in section III can be used, and the timing mismatch of each channel is calibrated to the average of the channel timing mismatches. And $\boldsymbol{B_x}$ can be calculated by (24). In order to estimate the error adaptively, we use the calibrated output $\hat{y}[n]$ to replace $y[n]$ in (34), and $y_i[(n\ mod\ M)] = y[n+i]$, then $y_{i+1}[(n\ mod\ M)] = y[n+i+1]$. Then τ_i can be expressed as $R_{\hat{y}[n+i]}(-1) - R_{\hat{y}[n+i]}(1)$. Simplifying further, $\tau_i = E\left[\hat{y}[n+i]\cdot\left(\hat{y}[n+i] - \hat{y}[n+i-1]\right)\right]$ can be obtained. So, the subtractor can be used in advance to get τ_i. The estimated structure is shown in Fig. 5, τ_i can be obtained by downsampling. Since $\boldsymbol{B}$ has only $M-1$ rows, we can not calculate τ_0, so the dashed part in Fig. 5 is not needed in the actual circuit. The ACC module is the accumulator required by the iterative algorithm in (39), [27]. The Avg module is a moving average filter, which can be expressed as [27]

$$s[n] = \frac{N-1}{N}s[n] + \frac{1}{N}q[n] \tag{41}$$

where $s[n]$ is the output, $q[n]$ is the input and $1/N$ is the weighting coefficient of the moving average.

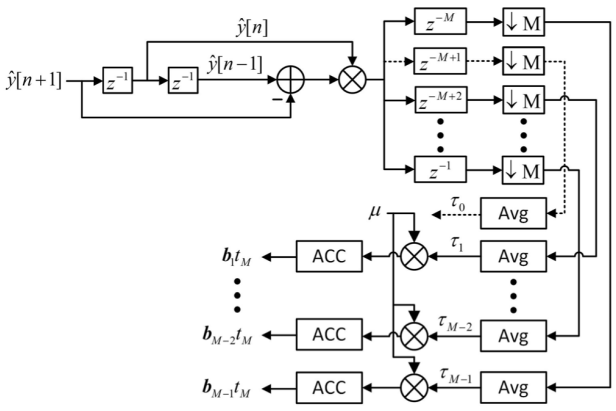

Fig. 5. The estimated structure.

V. Simulation and Hardware Implementation

We now demonstrate several engineering aspects of our calibration method, using numerical experiments and hardware implementation.

To deliberately evaluate the performance of the proposed calibration method (see Fig. 3 and Fig. 4) we take a 4-channel 12-bit TIADC for example to simulate the calibration module with the coefficient matrix generated directly by the MATLAB Function for the three cases, one absolute calibration case and two relative calibration cases.

Then we combine the calibration method with two representative estimation methods, the correlation function estimation and the estimation based on the statistical characteristics between adjacent channels respectively, to form a complete TIADC system and show the efficiency of the calibration structure by simulations, including examples from the literature.

A. Three Calibration Examples With Specified Coefficient Matrix

A 4-channel 12-bit TIADC is designed to simulate these three cases separately. Assuming that there is only quantization noise, the structures of Fig. 3 and Fig. 4 are used for absolute calibration and relative calibration, respectively. The timing mismatch values of four channels are $0.005T_s$, $-0.008T_s$, $0.01T_s$ and $0.013T_s$, respectively. The derivative FIR filter $H_d\left(e^{j\omega}\right)$ is generated by using the 'filterDesigner' tool in MATLAB and the filter order is 30. The estimation results $\boldsymbol{At_M}$ and $\boldsymbol{Bt_M}$ are obtained by using the MATLAB Function.

1) Absolute Calibration: In order to simply demonstrate the effectiveness of absolute calibration, the 4th order Hadamard matrix is used as the coefficient matrix, the coefficient matrix $\boldsymbol{A}$ is

$$\boldsymbol{A} = \begin{bmatrix} 1 & 1 & 1 & 1 \\ 1 & -1 & 1 & -1 \\ 1 & 1 & -1 & -1 \\ 1 & -1 & -1 & 1 \end{bmatrix}. \tag{42}$$

Then the corresponding modulation matrix $\boldsymbol{A_x}$ is calculated by (14),

$$\boldsymbol{A_x} = \begin{bmatrix} 0.25 & 0.25 & 0.25 & 0.25 \\ 0.25 & -0.25 & 0.25 & -0.25 \\ 0.25 & 0.25 & -0.25 & -0.25 \\ 0.25 & -0.25 & -0.25 & 0.25 \end{bmatrix}. \tag{43}$$

2) First Case of Relative Calibration: For the first case of relative calibration, we randomly generated a coefficient matrix $\boldsymbol{B}$ conforming to (28), and the coefficient matrix $\boldsymbol{B}$ is

$$\boldsymbol{B} = \begin{bmatrix} 1 & 0 & 1 & -2 \\ -1 & -1 & 3 & -1 \\ 2 & -3 & -2 & 3 \end{bmatrix}. \tag{44}$$

The modulation matrix $\boldsymbol{B_x}$ of the first case can be obtained according to (24), and

$$\boldsymbol{B_x} = \begin{bmatrix} 0.375 & -0.0625 & 0 & -0.3125 \\ -0.125 & -0.1875 & 0.25 & 0.0625 \\ 0.125 & -0.1875 & 0 & 0.0625 \end{bmatrix}. \tag{45}$$

3) Second Case of Relative Calibration: The coefficient matrix $\boldsymbol{B}$ of the second case is the same as (44). Since the calibration target is different from the first case, the modulation matrix $\boldsymbol{B_x}$ is obtained by (32),

$$\boldsymbol{B_x} = \begin{bmatrix} 0 & -0.4375 & -0.375 & -0.6875 \\ 0 & -0.0625 & 0.375 & 0.1875 \\ 0 & -0.3125 & -0.125 & -0.0625 \end{bmatrix}. \tag{46}$$

The calibration performance of the absolute calibration and the two cases of relative calibration are shown in Fig. 6.

Fig. 6(a) shows the spectrum of the uncalibrated input signal, and the SFDR is 40.36dB. Fig. 6(b) shows the output signal spectrum using the absolute calibration method. The coefficient matrix and the modulation matrix are (42) and (43) respectively. The SFDR of the output spectrum is 77.69dB. The output spectrum of the first case in the relative calibration is shown in Fig. 6(c). In the first case of relative calibration, the coefficient matrix and the modulation matrix are (44) and (45), respectively. As shown in Fig. 6(c), the SFDR of the output signal is calibrated to 77.1dB. The output spectrum of the second case in the relative calibration is shown in Fig. 6(d). The modulation matrix in the second case is (46), and the calibrated SFDR is 77.1dB. It can be seen that the calibration performance of the three calibration cases is almost the same, and all of them can effectively calibrate the timing mismatch. However, the calibration targets of the three calibration cases are different.

Absolute calibration makes the error approximately 0 ($\Delta t_i = 0$). Since the designed derivative FIR filter is not an ideal filter, there is a slight error between the output result of the absolute calibration and the signal without mismatch. The relative calibration is equivalent to the overall delay of the input signal.

Fig. 7 demonstrates the effectiveness of the three calibration methods from the time domain. And for the convenience of verification, the timing mismatch values of four channels are $-0.01T_s$, $0.006T_s$, 0 and $0.008T_s$, respectively. Fig. 7 depicts the time domain diagrams of the signal without mismatch and the output results of the three calibration methods. The output result of absolute calibration ('*Absolute Cal.*' in the legend) is close to the signal without mismatch ('*w/o mismatch*' in the legend). In the first case of relative calibration ('*Relatively 1) Cal.*' in the legend), the timing mismatches are all calibrated to the average value ($\Delta t_i = 0.001T_s$). In the second case ('*Relatively 2) Cal.*' in the legend), all channel errors are

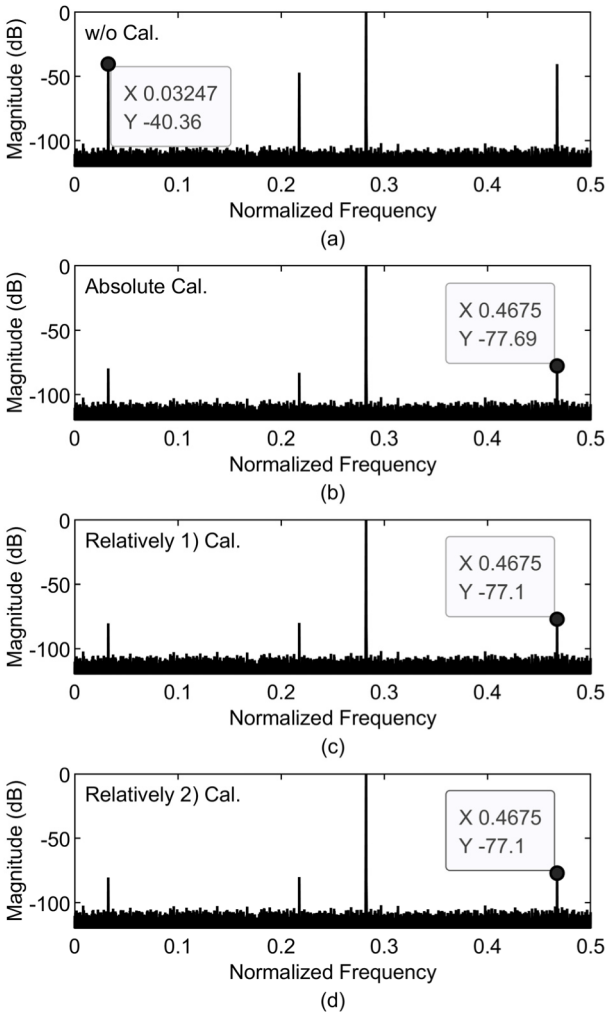

Fig. 6. The uncalibrated spectrum and spectrum after three types of calibration. (a) Input signal without calibration. (b) The output spectrum in the absolute calibration. (c) The output spectrum of the first case in the relative calibration. (d) The output spectrum of the second case in the relative calibration.

calibrated to be the same as the reference channel. If the channel of ADC_0 is the reference channel, then $\Delta t_i = -0.01T_s$. In Fig. 7, the time shift of the curve of *Relatively 1)* relative to the curve without mismatch is small, while the time shift of the curve of *Relatively 2)* relative to the curve without mismatch is larger. And the time shift direction of the two curves relative to the curve without mismatch is opposite. The theoretical analysis and simulation results are consistent. Therefore, it can be proved that the three methods can be effectively calibrated.

B. Simulation Result With Estimation Module

To illustrate the superiority of the calibration method, we combine the estimation method for further verification. Since the absolute and relative calibration have the same effect, and the relative calibration is more efficient in terms of practical implementation and has a wider application, we respectively use two representative estimation modules to combine our two relative calibration modules.

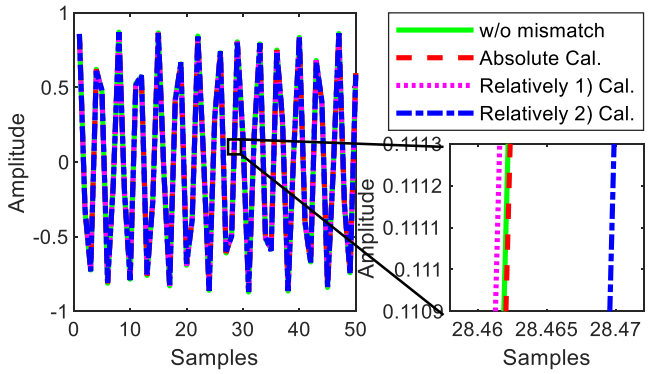

Fig. 7. The partial time domain plots for the signal without mismatch and the output results of three calibration methods.

1) The First Case of the Relative Calibration With Correlation Function Estimation: A four-channel, 12-bit TIADC system is designed. Assume that the TIADC system only has timing mismatch and quantization error. The timing mismatch values of four channels are set as $-0.004T_s$, $0.006T_s$, $-0.01T_s$ and $0.012T_s$, respectively. In the estimation module, considering the convergence time, signal-to-noise ratio, and hardware consumption, the iteration coefficient μ is set as $-1/2^8$, and the weighting coefficient of the moving average $1/N$ is set as $1/2^8$. The order of the derivative FIR filter is 30.

Combined with the estimation method based on the correlation function, the four-channel TIADC is simulated, and the coefficient matrix $\boldsymbol{B}$ is

$$\boldsymbol{B} = \begin{bmatrix} -1 & 2 & -1 & 0 \\ 0 & -1 & 2 & -1 \\ -1 & 0 & -1 & 2 \end{bmatrix}. \tag{47}$$

And the timing mismatches of all channels are calibrated to the average value for the first case of the relative calibration. Therefore, the corresponding modulation matrix $\boldsymbol{B_x}$ can be obtained from (24) and (47)

$$\boldsymbol{B_x} = \begin{bmatrix} -0.375 & 0.375 & 0.125 & -0.125 \\ -0.5 & 0 & 0.5 & 0 \\ -0.375 & -0.125 & 0.125 & 0.375 \end{bmatrix}. \tag{48}$$

Since the value in $\boldsymbol{B_x}$ is constant, we can decompose the elements in $\boldsymbol{B_x}$ to avoid the use of multipliers and get

$$\boldsymbol{B_x} = \frac{1}{8}\begin{bmatrix} -(1+2) & 1+2 & 1 & -1 \\ -4 & 0 & 4 & 0 \\ -(1+2) & -1 & 1 & 1+2 \end{bmatrix}. \tag{49}$$

It can be seen from (49) that shift and addition operations can be used to replace the multiplication required for modulation, which implies a significant saving in hardware resource consumption.

Fig. 8 shows the frequency spectrum before and after calibration when a multitone input signal is set as input. The SNR and SFDR before calibration are 38.12dB and 36.55dB, respectively. After calibration, the SNR and SFDR are 63.43dB and 75.07dB, respectively. Fig. 9 shows the convergence curve of the coefficients formed by the linear combination of the timing mismatch of each channel in the

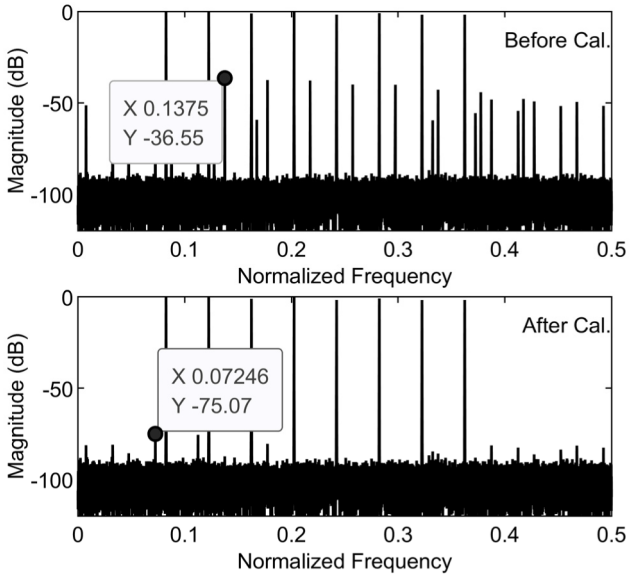

Fig. 8. The spectrum before and after calibration.

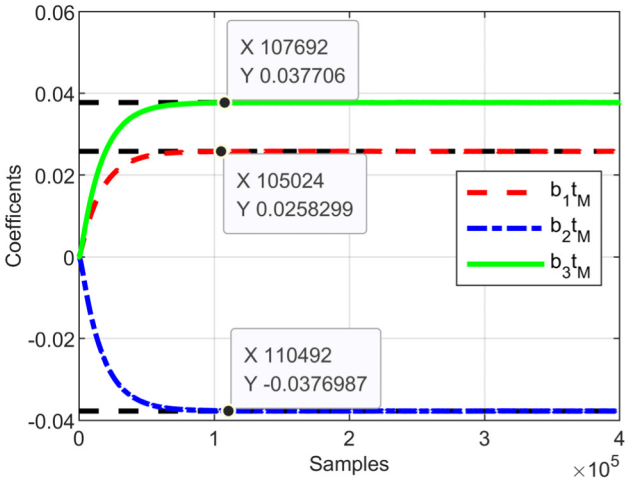

Fig. 9. Coefficients convergence curve.

estimation module. In Fig.9, the three coefficients $\boldsymbol{b_1 t_M}$, $\boldsymbol{b_2 t_M}$ and $\boldsymbol{b_3 t_M}$ converge to 0.02583, -0.0377 and 0.0377, respectively. Compared with the $\boldsymbol{Bt_M}$ calculation results 0.026, -0.038 and 0.038, the error is about 1%.

Fig. 10 shows the calibration performance of the proposed calibration method for the 12-bit four-channel TIADC in the range of normalized input frequency. SNR can be improved by about 24 to 35dB, and SFDR can be improved by about 35 to 45dB.

2) The Second Case of the Relative Calibration With Estimation Based on the Statistical Characteristics Between Adjacent Channels: In the second case, we still use the four-channel, 12-bit TIADC system designed in the first case of the relative calibration, and the timing mismatch values of four channels are set as $0.002T_s$, $0.01T_s$, $-0.008T_s$ and $0.015T_s$. For the estimation module, the iteration coefficient μ is set as $-1/2^{11}$, and the weighting coefficient of the moving

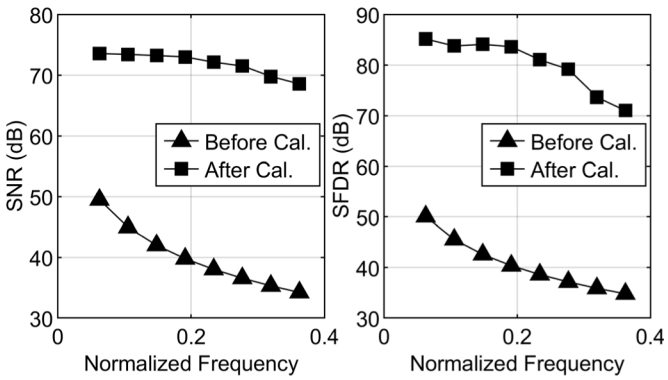

Fig. 10. Calibration performance (SNR and SFDR) vs. normalized input frequency.

average $1/N$ is set as $1/2^{11}$. Other simulation conditions are the same as the first case.

The goal of the second case of the relative calibration is to calibrate the timing mismatches of all channels to be same with one of them specified as the reference channel. Here, we set the first channel as the reference channel.

Combined with the estimation method based on the statistical characteristics between adjacent channels, the four-channel TIADC is simulated, and the coefficient matrix $\boldsymbol{B}$ is

$$\boldsymbol{B} = \begin{bmatrix} -1 & 2 & -1 & 0 \\ -1 & 0 & 1 & 0 \\ -1 & 0 & -1 & 2 \end{bmatrix}. \tag{50}$$

We use the modulation matrix to calibrate the timing mismatch of each channel to be the same as the first channel, and the modulation matrix can be obtained from (32)

$$\boldsymbol{B_x} = \begin{bmatrix} 0 & 0.5 & 0 & 0 \\ 0 & 0.5 & 1 & 0.5 \\ 0 & 0 & 0 & 0.5 \end{bmatrix}. \tag{51}$$

The right shift operation can be used to replace the operation of multiplying by 0.5 in the $\boldsymbol{B_x y_{d,M}}$ term. There is almost no consumption of hardware resources.

To compare our calibration method with the method in [26], we simulated the method in [26] and the method proposed in this paper respectively, under the same input frequency, derivative filter and iterative coefficients. The error convergence curve is shown in Fig. 11.

Fig. 11(a) shows the error convergence curve of the estimation method in [26]. For the four sub-ADCs of the four-channel, 12-bit TIADC system, the previous method [26] first uses ADC_0 to calibrate ADC_2. After the calibration of ADC_2 is completed, the ADC_2 and ADC_0 are used to calibrate ADC_1 and ADC_3. The error estimation of ADC_1 and ADC_3 depends on ADC_2, so the convergence speed of these two channels will be relatively slow. The 'Overshoot' in the convergence curve of ADC_1 and ADC_3 indicates that the calibration of ADC_1 and ADC_3 will be affected by the calibration process of ADC_2. The slowest convergence rate is ADC_1 in Fig. 11(a).

Fig. 11(b) shows the error convergence curve calibrated by combining the estimation method of [26] and the calibration structure of this paper. After combining the method of this

TABLE I
COMPARISON WITH OTHER METHODS

	[26] 2017 VLSI	[35] 2019 TCAS-II	[34] 2021 VLSI	[29] 2019 TCAS-I	[33] 2018 TCAS-I	[36] 2021 TCAS-I	Proposed method
Resolution	12	10	12	12	N/A	12	12
Channels	4	4	4	8	4	16	4
Mismatch type	Timing	Timing	Timing	Timing	Offset, Gain, Timing	Offset, Gain, Timing	Timing
Mismatch correction	Digital	Digital	Analog	Digital	Digital	Digital	Digital
Arbitrary channel	No	No	Yes	Yes	Yes	Yes	Yes
Step-by-step calibration	Yes	Yes	No	No	No	No	No
Matrix operation	No	No	No	Yes	No	No	No
Filter #	1	1	N/A	3	2	1	1
Filter taps	33	15	N/A	9+25+10	31	33	31
Conv. time (sample #)	N/A	80k	204.8k	3276k	40k	1200k	110k
Adder #	N/A	N/A	N/A	N/A	(M-1)(2L+4) +L-1	5M-1+L-1	4(M-1)+1+L-1
Multiplier #	N/A	N/A	N/A	N/A	(M-1)(2L+8) +L	5M-1+L	2(M-1)+1+L
SFDR /SNR(SNDR) improvement (dB)	-/29.03	24.2/19	44.6/27.8	32.1/-	40/30	40/-	38.52 /25.31

M: channel number, L: filter length

paper, the overshoot is eliminated, and the error estimation process of each channel is independent of each other. Through the comparison of Fig. 11 (a) and Fig. 11 (b), it can be clearly seen that the coefficients in Fig. 11 (b) converge faster, the estimation speed of ADC_1 and ADC_3 is increased by up to 65%, and the overall convergence speed is increased by 27%. The convergence value of the timing mismatch of ADC_2 in Fig. 11 (a) is $\Delta t_2 - \Delta t_0$, which is the same as the result of $\boldsymbol{b_2 t_M}$. Therefore, the timing mismatch of ADC_2 is not accelerated, but the overall estimation speed is improved. The proposed calibration method can significantly improve the convergence speed of the estimation method based on the statistical characteristics between adjacent channels.

Table I shows the comparison results with other methods. The method proposed by [33] can calibrate offset, gain and timing mismatch, but it requires the Hilbert filter and modulation of the signal, which requires more hardware resources. The method in [26] and [35] need to divide the calibration into several steps and perform the calibration step by step, and only apply to an even number of channels. The method in [34] can be used for multi-channel, but it needs to calculate the correlation function and consume a lot of hardware resources to get the value of the timing mismatch. The technique in [29] does not require step-by-step calibration, but needs matrix operations and a longer convergence time to obtain the high-accuracy mismatch value for each channel. Spectral information can be used to calibrate offset, gain, and timing mismatch [36], but requires a large number of multipliers and adders to implement discrete Fourier transforms. Compared with other works, our proposed method does not need to perform calibration in steps, and the error convergence time is not long. Moreover, it eliminates the need for matrix operations which is used to obtain the value of the timing mismatch, and saves hardware resources.

C. Hardware Implementation

The fixed-point model for a four-channel TIADC, which incorporates the structure of Fig. 4 and Fig. 5, is designed in MATLAB-Simulink with a sampling rate at 500MS/s and 12-bit resolution. The multi-tone input signal with frequencies of 51, 71, 91, 111, 141, 171 MHz, respectively, is generated by the fixed-point Simulink model in MATLAB, which has non-ideal effects, including the timing mismatch, and the quantization noise. The modulation matrix is the same as (49). According to the optimization of the fixed-point simulation, the order of the derivative filter is set as 30. The tap coefficients of derivative filter are presented with 16-bit signed fixed-point data with fractional bits of 15. Both the outputs of the multipliers and adders in the derivative filter are presented with 16-bit signed fixed-point data with fractional bits of 15. To obtain a better calibration effect, for the estimation module, the signal path Word-Length for the multiplier is 31 bits with fractional bits of 30 and the signal path Word-Length for the moving average filter is 32 bits with fractional bits of 31. According to the final convergence result, the output Word-Length of the accumulator is truncated to 16 bits with fractional bits of 15. At last, the calibrated output is rounded to 12 bits with fractional bits of 11.

After the optimization of the fixed-point simulation, the proposed TIADC calibration structure is designed by Verilog hardware description language (HDL). The output of RTL simulations in Modelsim is identical to the output of MATLAB Simulink simulations. Thus, we use Virtex

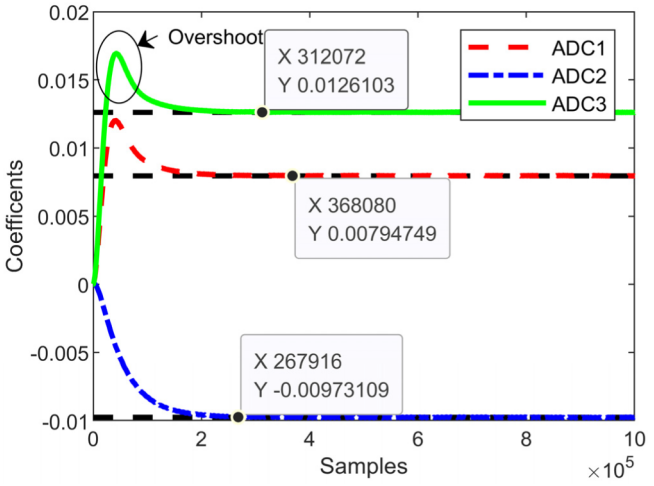

(a) Use the method in [26] directly

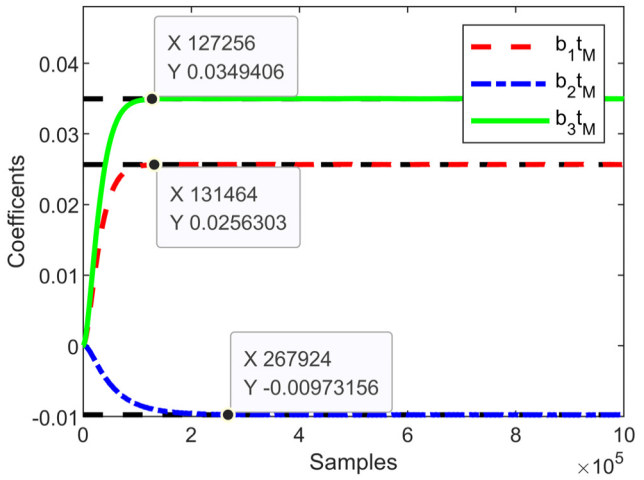

(b) Combine the estimation method in [26] with the proposed calibration structure

Fig. 11. Convergence of the mismatch estimate for two calibration structure.

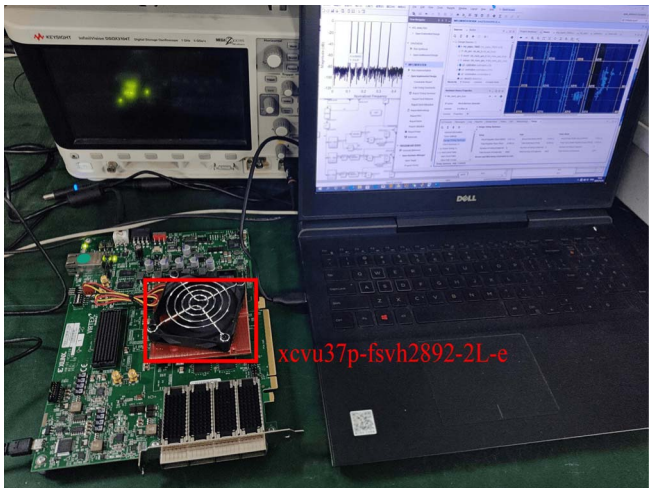

Fig. 12. FPGA validation platform.

UltraScale+ HBM VCU128 Evaluation Platform (xcvu37p-fsvh2892-2L-e) for hardware implementation. Fig.12 shows the verification platform. We save the uncalibrated TIADC output data in BRAM in advance. When the reset button on the evaluation platform is pressed, BRAM sends data to the calibration system. At the same time, the calibrated data is sent to the PC for spectrum analysis through MATLAB. Fig. 13 shows the output spectrum before and after calibration. Comparing the spectrum before and after calibration, the SFDR has been increased from 36.64dB before calibration to 74.27dB after calibration. The resource utilization of implementation is shown in Table II. The design only uses a few hardware resources to complete the calibration. The Verilog HDL design is also synthesized to a gate-level netlist using a Synopsys Design Compiler (DC) targeting the 55nm 1.2V CMOS logic technology. The overall clock speed of the calibration circuit is 1GHz. It consumes about total power of 28.13mW and occupies an area of 0.0472mm^2. The synthesized calibration system uses 25780 cells in total as shown in Table III.

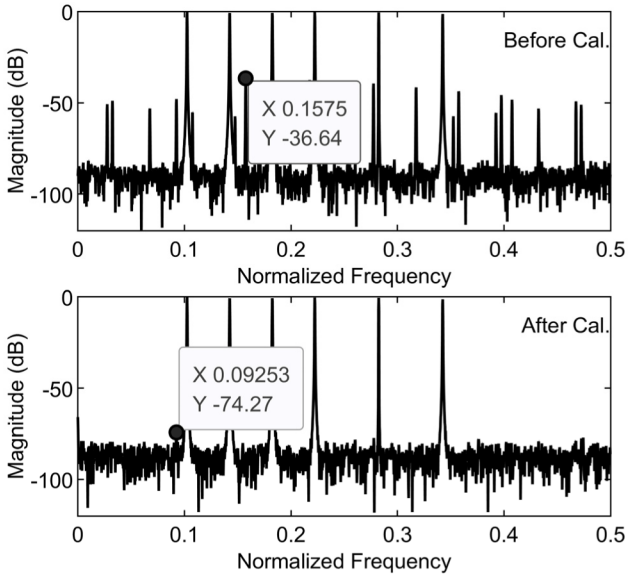

Fig. 13. Output spectrum before and after calibration.

TABLE II
RESOURCE UTILIZATION

Resource	Utilization	Available	Utilization %
LUT	2197	1303680	0.17
LUTRAM	204	600960	0.03
FF	1620	2607360	0.06
DSP	50	9024	0.6

TABLE III
SYNTHESIS RESULTS

Type	Cells	Area [μm^2]	Area %
Combinational	18519	30696.4	65.01
Sequential	2505	16518.6	34.99
Buf/Inv	4756	4584.44	9.71
Total	25780	47215	100

VI. Conclusion

A new all-digital calibration method based on the modulation matrix is proposed to calibrate the timing mismatch in TIADC. Based on the concepts of modulation matrix and coefficient matrix, the inductive expression of the calibration method is derived, which can be used to guide the design of TIADC calibration. According to the coefficient matrix obtained by different estimation methods, different modulation matrices can be derived to modulate the signal. This method can avoid the multiplication of the pseudo-inverse matrix and the estimation result. Therefore, the hardware complexity can be reduced. When using the estimation method based on the statistical characteristics between adjacent channels, the proposed method can make the estimation process of each channel independent of each other and improve the estimation speed. In addition, the conditions under which the modulation matrix can be obtained are also derived. The simulation results of 12-bit four-channel show that when multi-tone input, the calibrated SFDR is 75.07dB, and the SNR is 63.43dB. This method is also implemented in hardware, and the output SFDR is improved by 37.63dB.

References

[1] C. Vogel, "The impact of combined channel mismatch effects in time-interleaved ADCs," *IEEE Trans. Instrum. Meas.*, vol. 54, no. 1, pp. 415–427, Feb. 2005.

[2] N. L. Dortz *et al.*, "A 1.62 GS/s time-interleaved SAR ADC with digital background mismatch calibration achieving interleaving spurs below 70 dBFS," in *IEEE ISSCC Dig. Tech. Papers*, Feb. 2014, pp. 386–388.

[3] D. Xing *et al.*, "Seven-bit 700-MS/s four-way time-interleaved SAR ADC with partial V_{cm}-based switching," *IEEE Trans. Very Large Scale Integr. (VLSI) Syst.*, vol. 25, no. 3, pp. 1168–1172, Mar. 2017.

[4] M. Guo, J. Mao, S. W. Sin, H. Wei, and R. P. Martins, "A 1.6-GS/s 12.2-mW seven-/eight-way split time-interleaved SAR ADC achieving 54.2-dB SNDR with digital background timing mismatch calibration," *IEEE J. Solid-State Circuits*, vol. 55, no. 3, pp. 693–705, Mar. 2020.

[5] B. Razavi, "Design considerations for interleaved ADCs," *IEEE J. Solid-State Circuits*, vol. 48, no. 8, pp. 1806–1817, Aug. 2013.

[6] J. Li *et al.*, "A digital timing mismatch calibration technique in time-interleaved ADCs," *IEEE Trans. Circuits Syst. II, Exp. Briefs*, vol. 61, no. 7, pp. 486–490, Jul. 2014.

[7] K. C. Dyer, J. P. Keane, and S. Lewis, "Calibration and dynamic matching in data converters: Part 2: Time-interleaved analog-to-digital converters and background-calibration challenges," *IEEE Solid State Circuits Mag.*, vol. 10, no. 3, pp. 61–70, May 2018.

[8] S. J. Liu, P. P. Qi, J. S. Wang, M. H. Zhang, and W. S. Jiang, "Adaptive calibration of channel mismatches in time-interleaved ADCs based on equivalent signal recombination," *IEEE Trans. Instrum. Meas.*, vol. 63, no. 2, pp. 277–286, Feb. 2014.

[9] M. I. Nassiri and M. Rezvanyvardom, "A new adaptive blind background calibration of gain and timing mismatch for a two-channel time-interleaved ADC," *Microelectron. J.*, vol. 77, pp. 26–33, Jul. 2018.

[10] S. Tertinek and C. Vogel, "Reconstruction of two-periodic nonuniformly sampled band-limited signals using a discrete-time differentiator and a time-varying multiplier," *IEEE Trans. Circuits Syst. II, Exp. Briefs*, vol. 54, no. 7, pp. 616–620, Jul. 2007.

[11] S. Tertinek and C. Vogel, "Reconstruction of nonuniformly sampled bandlimited signals using a differentiator–multiplier cascade," *IEEE Trans. Circuits Syst. I, Reg. Papers*, vol. 55, no. 8, pp. 2273–2286, Sep. 2008.

[12] J. Matsuno, T. Yamaji, M. Furuta, and T. Itakura, "All-digital background calibration technique for time-interleaved ADC using pseudo aliasing signal," *IEEE Trans. Circuits Syst. I, Reg. Papers*, vol. 60, no. 5, pp. 1113–1121, May 2013.

[13] Y. T. Qiu, J. Zhou, Y. J. Liu, G. F. Zhang, and Y. N. Liu, "Novel adaptive blind calibration technique of time-skew mismatches for any channel time-interleaved analogue-to-digital converters," *IET Circuits, Devices Syst.*, vol. 13, no. 6, pp. 830–835, Sep. 2019.

[14] H. Johansson, "A polynomial-based time-varying filter structure for the compensation of frequency-response mismatch errors in time-interleaved ADCs," *IEEE J. Sel. Topics Signal Process.*, vol. 3, no. 3, pp. 384–396, Jun. 2009.

[15] H. Johansson and P. Lowenborg, "Reconstruction of nonuniformly sampled bandlimited signals by means of digital fractional delay filters," *IEEE Trans. Signal Process.*, vol. 50, no. 11, pp. 2757–2767, Nov. 2002.

[16] S. Huang and B. C. Levy, "Blind calibration of timing offsets for four-channel time-interleaved ADCs," *IEEE Trans. Circuits Syst. I, Reg. Papers*, vol. 54, no. 4, pp. 863–876, Apr. 2007.

[17] T. H. Tsai, P. J. Hurst, and S. H. Lewis, "Correction of mismatches in a time-interleaved analog-to-digital converter in an adaptively equalized digital communication receiver," *IEEE Trans. Circuits Syst. I, Reg. Papers*, vol. 56, no. 2, pp. 307–319, Feb. 2009.

[18] S. Liu, H. Ma, N. Lyu, and H. Wang, "Adaptive blind timing mismatch calibration with low power consumption in M-channel time-interleaved ADC," *Circuits, Syst., Signal Process.*, vol. 37, no. 11, pp. 4861–4879, Nov. 2018.

[19] C. Vogel, S. Saleem, and S. Mendel, "Adaptive blind compensation of gain and timing mismatches in M-channel time-interleaved ADCs," in *Proc. 15th IEEE Int. Conf. Electron., Circuits Syst.*, Aug. 2008, pp. 49–52.

[20] S. Liu, N. Lyu, J. Cui, and Y. Zou, "Improved blind timing skew estimation based on spectrum sparsity and ApFFT in time-interleaved ADCs," *IEEE Trans. Instrum. Meas.*, vol. 68, no. 1, pp. 73–86, Jan. 2019.

[21] C.-Y. Lin, Y.-H. Wei, and T.-C. Lee, "A 10-bit 2.6-GS/s time-interleaved SAR ADC with a digital-mixing timing-skew calibration technique," *IEEE J. Solid-State Circuits*, vol. 53, no. 5, pp. 1508–1517, May 2018.

[22] D.-J. Chang, M. Choi, and S.-T. Ryu, "A 28-nm 10-b 2.2-GS/s 18.2-mW relative-prime time-interleaved sub-ranging SAR ADC with on-chip background skew calibration," *IEEE J. Solid-State Circuits*, vol. 56, no. 9, pp. 2691–2700, Sep. 2021.

[23] M. Guo *et al.*, "A 5 GS/s 29 mW interleaved SAR ADC with 48.5 dB SNDR using digital-mixing background timing-skew calibration for direct sampling applications," *IEEE Access*, vol. 8, pp. 138944–138954, 2020.

[24] A. Abbaszadeh, E. N. Aghdam, and A. Rosado-Muñoz, "Low complexity digital background calibration algorithm for the correction of timing mismatch in time-interleaved ADCs," *Microelectron. J.*, vol. 83, pp. 117–125, Jan. 2019.

[25] X. Li, J. Wu, and C. Vogel, "A background correlation-based timing skew estimation method for time-interleaved ADCs," *IEEE Access*, vol. 9, pp. 45730–45739, 2021.

[26] S. Chen, L. Wang, H. Zhang, R. Murugesu, D. Dunwell, and A. C. Carusone, "All-digital calibration of timing mismatch error in time-interleaved analog-to-digital converters," *IEEE Trans. Very Large Scale Integr. (VLSI) Syst.*, vol. 25, no. 9, pp. 2552–2560, Sep. 2017.

[27] S. Liu, L. Zhao, Z. Deng, and Z. Zhang, "A digital adaptive calibration method of timing mismatch in TIADC based on adjacent channels Lagrange mean value difference," *Circuits, Syst., Signal Process.*, vol. 40, no. 12, pp. 6301–6323, Dec. 2021.

[28] H. L. Duc, D. M. Nguyen, C. Jabbour, P. Desgreys, O. Jamin, and V. T. Nguyen, "Fully digital feedforward background calibration of clock skews for sub-sampling TIADCs using the polyphase decomposition," *IEEE Trans. Circuits Syst. I, Reg. Papers*, vol. 64, no. 6, pp. 1515–1528, Jun. 2017.

[29] A. Salib, M. F. Flanagan, and B. Cardiff, "A high-precision time skew estimation and correction technique for time-interleaved ADCs," *IEEE Trans. Circuits Syst. I, Reg. Papers*, vol. 66, no. 10, pp. 3747–3760, Oct. 2019.

[30] M. Yin and Z. Ye, "First order statistic based fast blind calibration of time skews for time-interleaved ADCs," *IEEE Trans. Circuits Syst. II, Exp. Briefs*, vol. 67, no. 1, pp. 162–166, Jan. 2020.

[31] G. Strang, *Introduction to Linear Algebra*, 5th ed. Wellesley, MA, USA: Wellesley-Cambridge, 2016.

[32] H. Wei, P. Zhang, B. D. Sahoo, and B. Razavi, "An 8 bit 4 GS/s 120 mW CMOS ADC," *IEEE J. Solid-State Circuits*, vol. 49, no. 8, pp. 1751–1761, Aug. 2014.

[33] Y. Qiu, Y.-J. Liu, J. Zhou, G. Zhang, D. Chen, and N. Du, "All-digital blind background calibration technique for any channel time-interleaved ADC," *IEEE Trans. Circuits Syst. I, Reg. Papers*, vol. 65, no. 8, pp. 2503–2514, Aug. 2018.

[34] Z. Lu, H. Tang, Z. Ren, R. Hua, H. Zhuang, and X. Peng, "A timing mismatch background calibration algorithm with improved accuracy," *IEEE Trans. Very Large Scale Integr. (VLSI) Syst.*, vol. 29, no. 8, pp. 1591–1595, Aug. 2021.

[35] D. Li, Z. Zhu, R. Ding, M. Liu, Y. Yang, and N. Sun, "A 10-bit 600-MS/s time-interleaved SAR ADC with interpolation-based timing skew calibration," *IEEE Trans. Circuits Syst. II, Exp. Briefs*, vol. 66, no. 1, pp. 16–20, Jan. 2019.
[36] H. Niu and J. Yuan, "A spectral-correlation-based blind calibration method for time-interleaved ADCs," *IEEE Trans. Circuits Syst. I, Reg. Papers*, vol. 67, no. 12, pp. 5007–5017, Dec. 2020.

Sujuan Liu (Member, IEEE) received the B.S. degree in electronic engineering from Shandong University, Jinan, China, in 2001, and the Ph.D. degree in microelectronics and solid-state electronics from the Beijing University of Technology, Beijing, China, in 2006.

Since 2006, she has been with the College of Microelectronics, Beijing University of Technology, where she is currently an Associate Professor. She is involved in the time-interleaved analog-to-information converter research project. Her current research interests include design and implementation of analog-to-digital converters, mixed-signal systems, and digital signal processing.

Dr. Liu has been serving as an Evaluation/the Peer-Reviewed Expert for the National Natural Science Foundation of China since 2011 and also as the Paper Reviewer for several IEEE journals and international conferences.

Lin Zhao received the B.S. degree in electronic science and technology from the Beijing University of Technology, Beijing, China, in 2019, where he is currently pursuing the M.S. degree with the College of Microelectronics.

His current research interests include high-speed data conversion, digital signal processing, and system design.

Shibo Li received the B.S. degree in electronic engineering from the Beijing University of Technology, Beijing, China, in 2020, where he is currently pursuing the M.S. degree in electronic engineering.

His research interests include the area of high sampling systems, mainly focusing on the digital background calibration techniques of the TI-ADC systems.